J Supercond Nov Magn (2012) 25:1971–1977
DOI 10.1007/s10948-012-1545-x

ORIGINAL PAPER

Preparation of Magnetic $Cu_{0.5}Mg_{0.5}Fe_2O_4$ Nanoparticles and Kinetics of Thermal Process of Precursor

Jinwen Huang · Peng Su · Wenwei Wu · Yongni Li · Xuehang Wu · Sen Liao

Received: 19 January 2012 / Accepted: 26 March 2012 / Published online: 10 April 2012

Abstract $Cu_{0.5}Mg_{0.5}Fe_2O_4$ precursor was synthesized by solid-state reaction at low heat using $CuSO_4{\cdot}5H_2O$, $MgSO_4{\cdot}6H_2O$, $FeSO_4{\cdot}7H_2O$, and $Na_2C_2O_4$ as raw materials. The spinel $Cu_{0.5}Mg_{0.5}Fe_2O_4$ was obtained via calcining precursor above 300 °C in air. The precursor and its calcined products were characterized by thermogravimetry and differential scanning calorimetry (TG/DSC), Fourier transform FT-IR, X-ray powder diffraction (XRD), scanning electron microscopy (SEM), energy dispersive X-ray spectrometer (EDS), and vibrating sample magnetometer (VSM). The result showed that $Cu_{0.5}Mg_{0.5}Fe_2O_4$ obtained at 600 °C had a saturation magnetization of 36.8 emu g^{-1}. The thermal process of $Cu_{0.5}Mg_{0.5}Fe_2O_4$ precursor experienced two steps, which involved the dehydration of the five and a half crystal water molecules at first, and then decomposition of $Cu_{0.5}Mg_{0.5}Fe_2(C_2O_4)_3$ into crystalline $Cu_{0.5}Mg_{0.5}Fe_2O_4$ in air. Based on the Kissinger equation, the values of the activation energy associated with the thermal process of the precursor were determined to be 85 and 152 kJ mol^{-1} for the first and second thermal process steps, respectively.

Keywords $Cu_{0.5}Mg_{0.5}Fe_2O_4$ · Magnetic properties · Solid-state reaction at low heat · Thermal process · Non-isothermal kinetics

J. Huang · W. Wu (✉) · Y. Li · X. Wu · S. Liao
School of Chemistry and Chemical Engineering, Guangxi University, Nanning 530004, P.R. China
e-mail: gxuwuwenwei@yahoo.com.cn

J. Huang · P. Su
Guangxi Institute of Metallurgy, Nanning 530023, P.R. China

1 Introduction

Spinels of the type $M^{2+}M_2^{3+}O_4$ ($M^{2+} = Cu^{2+}$, Mn^{2+}, Mg^{2+}, Zn^{2+}, Ni^{2+}, Co^{2+}, etc.; $M^{3+} = Fe^{3+}$) have many unique properties, such as high electrical resistivity, high permeability, high Curie temperature, mechanical hardness, large magnetocrystalline anisotropy, high coercivity, chemical stability, and temperate specific saturation magnetization. Therefore, spinel ferrites have been extensively used in many fields, such as high-density information storage, catalysts, ferrofluids, drug targeting, magnetic separation, magnetic resonance imaging, and gas sensor [1–11]. Spinel ferrites have a cubic close-packed structure. The cation occupies two types of interstitial position. One of them is called a tetrahedral A-site with the cation surrounded by four oxygen ions forming tetrahedral coordination. The other interstitial position is known as octahedral B-site with the cation coordinated by six oxygen ions forming octahedral coordination. The ferrospinels can be depicted in the chemical formula $(M^{2+}_{1-\delta}Fe^{3+}_{\delta})[M^{2+}_{\delta}Fe^{3+}_{2-\delta}]O^{2-}_4$. Here the parentheses and square brackets denote A and B sites, respectively, M represent divalent cation and δ the inversion parameter [1]. The magnetic moment direction of cations in parentheses is opposite with that in square brackets. Therefore, magnetic as well as electrical properties of spinel ferrites depend on the distribution of cations at the different sites as well as preparation conditions. Copper ferrite ($CuFe_2O_4$) is very important soft magnetic material. Its properties, such as magnetic behavior and gas-sensing properties, are highly dependent on the synthesis method and doping elements.

To date, various methods have been developed to synthesize $CuFe_2O_4$ with cubic structure, including ball-milling [12, 13], sol–gel synthesis [14], coprecipitation [15, 16], combustion synthesis [17], microwave synthesis [18], solid-state reaction at low heat [4, 19], etc. In the synthesis of

$CuFe_2O_4$, it was found that crystallite diameter, morphology, and crystalline phases of $CuFe_2O_4$ associated with its properties were highly dependent on the synthesis method and temperature. For instance, Sun et al. [4] obtained spinel-type $CuFe_2O_4$ with a crystallite size of 75 nm by solid-state reaction at low heat when precursor was calcined at 600 °C. Tao et al. [16] studied synthesis of spinel-type $CuFe_2O_4$ via sol–gel and coprecipitation methods, respectively. The results showed that spinel-type $CuFe_2O_4$ was obtained at 600 °C via calcining precursor from coprecipitation method. However, pure $CuFe_2O_4$ was not obtained until 800 °C by a sol–gel process, which might be due to the loose contact between copper and iron ions and the possible low diffusion rate.

The doped copper ferrite can improve its performance. Therefore, doped copper ferrite has caused great concern, and some progress has been made. It is reported that substitutions of Cu^{2+} with other transition metals ions lead to improve magnetic properties and catalytic properties of nanocrystalline ferrites [20–25], such as when Cu^{2+} ions in spinel $CuFe_2O_4$ are partially substituted by Co^{2+}, $Cu_{1-x}Co_xFe_2O_4$ obtained by chemical coprecipitation shows that saturation magnetization of sample increases with Co percentage [20]. Banerjee et al. [23] synthesized $Zn_{1-x}Cu_xFe_2O_4$ ($x = 0.0, 0.25, 0.50, 0.75, 1.0$) by coprecipitation method, and studied their catalytic properties. The results showed that the conversion of pyridine increases with increasing copper content in $Zn_{1-x}Cu_xFe_2O_4$. However, synthesis research of doped $CuFe_2O_4$ still has fewer reports in comparison with that of $CuFe_2O_4$. Therefore, new synthesis methods for $Cu_{1-x}M_xFe_2O_4$ (M = transition metals or alkaline earth metals) still need to be studied and innovated further. Besides, the kinetics study of thermal process for $Cu_{1-x}M_xFe_2O_4$ precursor is important to obtain high-quality crystalline doped $CuFe_2O_4$ for practical applications.

The aim of this work is to prepare polycrystalline $Cu_{0.5}Mg_{0.5}Fe_2O_4$ using $CuSO_4{\cdot}5H_2O$, $MgSO_4{\cdot}7H_2O$, $FeSO_4{\cdot}7H_2O$, and $Na_2C_2O_4$ as raw materials via solid-state reaction at low heat [6, 11] and to study magnetic properties of $Cu_{0.5}Mg_{0.5}Fe_2O_4$, and kinetics of the thermal process of precursor. The kinetics of the thermal process of precursor was studied using TG-DSC techniques. Non-isothermal kinetics of the thermal process of precursor was interpreted by Kissinger equation [11, 26–28]. The kinetic parameters (E_a, A) of the thermal decomposition of $Cu_{0.5}Mg_{0.5}Fe_2O_4$ precursor are discussed for the first time.

2 Experimental

2.1 Reagent and Apparatus

All chemicals were of reagent grade purity (purity > 99.9 %). TG/DSC measurements were made using a Netsch 40PC thermogravimetric analyzer. X-ray powder diffraction (XRD) was performed using a Rigaku D/max 2500 V diffractometer equipped with a graphite monochromator and a Cu target. The FT-IR spectra of the precursor and its calcined products were recorded on a Nexus 470 FT-IR instrument. The morphologies of the calcined samples and energy dispersive X-ray spectrometer (EDS) were obtained on S-3400 scanning electron microscopy (SEM). The specific saturation magnetizations (M_s) of the calcined sample powders were carried out at room temperature using a magnetic property measurement system (SQUID-MPMS-XL-5).

2.2 Preparation of $Cu_{0.5}Mg_{0.5}Fe_2O_4$

The $Cu_{0.5}Mg_{0.5}Fe_2O_4$ precursor was prepared by solid-state reaction at low heat using $CuSO_4{\cdot}5H_2O$, $MgSO_4{\cdot}7H_2O$, $FeSO_4{\cdot}7H_2O$, and $Na_2C_2O_4$ as raw materials at first. In a typical synthesis, $CuSO_4{\cdot}5H_2O$ (12.25 g), $MgSO_4{\cdot}7H_2O$ (12.09 g), $FeSO_4{\cdot}7H_2O$ (54.54 g), $Na_2C_2O_4$(45.34 g), and surfactant polyethylene glycol (PEG)-400 (3.5 mL, 50 vol.%) were put in a mortar, and the mixture was fully ground by hand with a rubbing mallet at room temperature for 35 min. The grinding velocity was about 220 circles/min, and the strength applied was moderate. The reactant mixture gradually became damp, and then a paste formed quickly. The reaction mixture was kept at room temperature for 2 h. The mixture was washed with deionized water to remove soluble inorganic salts until SO_4^{2-} ion could not be visually detected with a 0.5 mol L^{-1} $BaCl_2$ solution. The solid was then washed with a small amount of anhydrous ethanol and dried at 75 °C for 6 h. The resulting material was subsequently determined to be $Cu_{0.5}Mg_{0.5}Fe_2(C_2O_4)_3{\cdot}5.5H_2O$. Nanocrystalline $Cu_{0.5}Mg_{0.5}Fe_2O_4$ with cubic structure was obtained via calcining $Cu_{0.5}Mg_{0.5}Fe_2(C_2O_4)_3{\cdot}5.5H_2O$ above 300 °C in air for 1 h.

3 Determination of Kinetic Parameters of Thermal Process

According to DSC curves and the Kissinger equation (Eq. (1)) [26], the activation energy of thermal process of the $Cu_{0.5}Mg_{0.5}Fe_2O_4$ precursor can be obtained,

$$\ln\frac{\beta}{T_P^2} = -\frac{E_a}{RT_P} + \ln\frac{AR}{E_a} \tag{1}$$

where β is the heating rate (K min^{-1}), T_P is the peak temperature (K) in DSC curve, E_a is the activation energy (kJ mol^{-1}) of thermal process, R is the gas constant (8.314×10^{-3} kJ mol^{-1} K^{-1}), and A is the pre-exponential factor. According to Eq. (1), the plot of $\ln(\beta/T_P^2)$ versus $1/T_P$ can be obtained by a linear regression of least-square

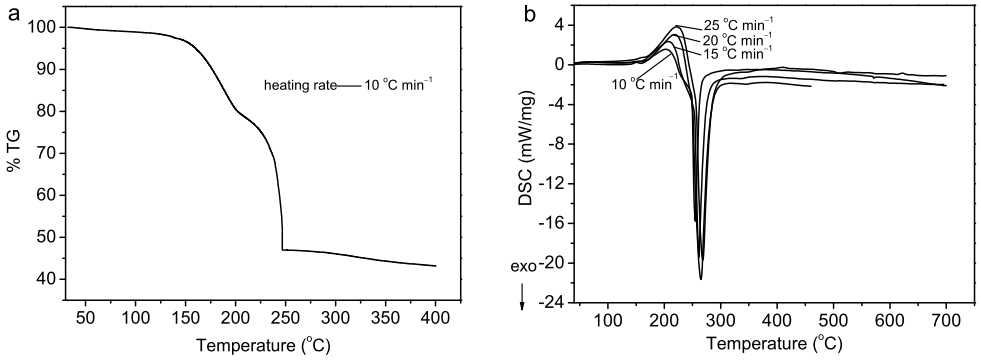

Fig. 1 TG/DSC curves of $Cu_{0.5}Mg_{0.5}Fe_2(C_2O_4)_3{\cdot}5.5H_2O$ at different heating rates in air

method. The dependence of $\ln(\beta/T_P^2)$ on $1/T_P$ must give a good linear relation. Thus, reaction activation energy E_a can be obtained from linear slope $(-E_a/R)$, and the pre-exponential factor A can be obtained from linear intercept $(\ln(AR/E_a))$.

4 Results and Discussion

4.1 TG/DSC Analysis of Precursor

Figure 1 shows the TG/DSC curves of the synthetic product at four different heating rates in air, respectively.

The TG/DSC curves show that thermal process of the $Cu_{0.5}Mg_{0.5}Fe_2(C_2O_4)_3{\cdot}5.5H_2O$ below 700 °C occurs in two well-defined steps. For heating rate of 10 °C min^{-1}, the first step starts at 50 °C, ends at 202 °C, and characterized by an endothermic DSC peak at about 202 °C, which can be attributed to dehydration of the five and a half crystal water molecules from $Cu_{0.5}Mg_{0.5}Fe_2(C_2O_4)_3{\cdot}5.5H_2O$ and formation of $Cu_{0.5}Mg_{0.5}Fe_2(C_2O_4)_3$. The observed mass loss in the TG curve is 19.53 %, which is in good agreement with 19.1 % theoretic mass loss of dehydration of the five and a half crystal water molecules from $Cu_{0.5}Mg_{0.5}Fe_2(C_2O_4)_3{\cdot}5.5H_2O$. The second decomposition step begins at 202 °C, and ends at 400 °C, which involves an exothermic process with a strong DSC peak at 255 °C, attributed to the decomposition of $Cu_{0.5}Mg_{0.5}Fe_2(C_2O_4)_3$ in air and formation of $Cu_{0.5}Mg_{0.5}Fe_2O_4$. The corresponding observed mass loss in the TG curve is 37.29 %, which close to 38.55 % theoretic mass loss of reaction of $Cu_{0.5}Mg_{0.5}Fe_2(C_2O_4)_3$ with two O_2 molecules. No other exothermic DSC peak that is ascribed to crystallization of $Cu_{0.5}Mg_{0.5}Fe_2O_4$, which indicates that exothermic DSC peak of crystallization of $Cu_{0.5}Mg_{0.5}Fe_2O_4$ is overlapped with that from decomposition of $Cu_{0.5}Mg_{0.5}Fe_2(C_2O_4)_3$. The peak temperature of thermal process is the temperature at which it attains its maximum. From Fig. 1b, there is an upward shift in T_P with increasing heating rate, peak temperatures from heating rate of 10, 15, 20, and 25 °C min^{-1} are 202, 209, 216, and 221 °C for first step, and 255, 261, 266, and 268 °C for second step, respectively.

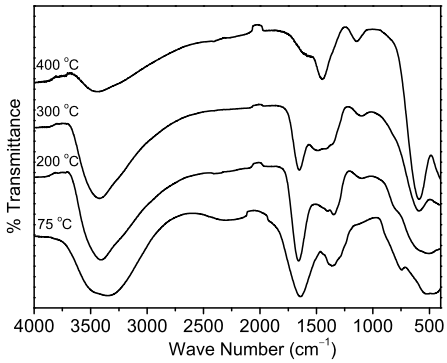

Fig. 2 FT-IR spectra of $Cu_{0.5}Mg_{0.5}Fe_2(C_2O_4)_3{\cdot}5.5H_2O$ and its calcined samples

4.2 IR Spectroscopic Analysis of $Cu_{0.5}Mg_{0.5}Fe_2(C_2O_4)_3{\cdot}5.5H_2O$ and Its Calcined Samples

The FT-IR spectra of $Cu_{0.5}Mg_{0.5}Fe_2(C_2O_4)_3{\cdot}5.5H_2O$ and of its calcined sample are shown in Fig. 2.

The $Cu_{0.5}Mg_{0.5}Fe_2(C_2O_4)_3{\cdot}5.5H_2O$ exhibits a strong and broad band at about 3393 cm^{-1} that can be assigned to the stretching OH vibration of the water molecule. The strong band which appears at 1647 cm^{-1} in the spectrum of the precursor can be ascribed to the bending mode of the HOH. The bands at 1356 cm^{-1} can be assigned to either the appearance of new M–OC_2O_3 (M = Cu, Mg, Fe) bonds and/or to the combinations of OH librations and lattice modes [6, 11, 19, 29]. The band at 1356 cm^{-1} shifts to 1444 cm^{-1} when sample is calcined at 400 °C, which indicates that $Cu_{0.5}Mg_{0.5}Fe_2(C_2O_4)_3$ finishes the decomposition of $C_2O_4^{2-}$. The absorption band of the samples obtained above 300 °C, which appears at about 3400 cm^{-1}, is attributed to the adsorption of water from air.

4.3 XRD Analysis of $Cu_{0.5}Mg_{0.5}Fe_2(C_2O_4)_3{\cdot}5.5H_2O$ and Its Calcined Samples

Figure 3 shows the XRD patterns of $Cu_{0.5}Mg_{0.5}Fe_2(C_2O_4)_3{\cdot}5.5H_2O$ dried at 75 °C and the products resulting from calcination at different temperatures in air for 1 h.

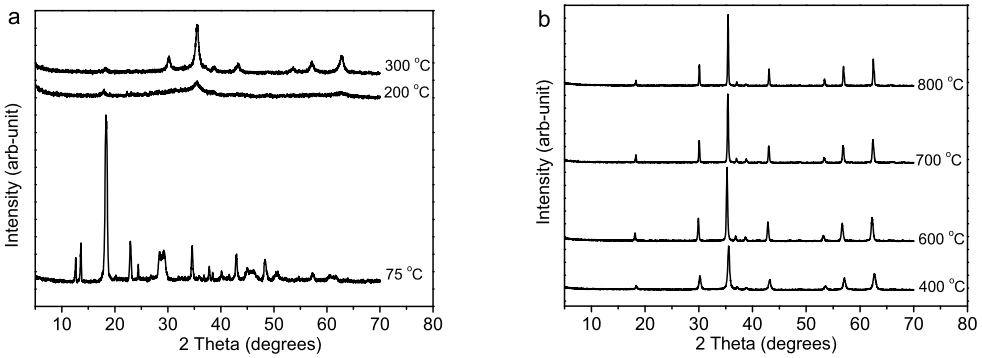

Fig. 3 XRD patterns of $Cu_{0.5}Mg_{0.5}Fe_2(C_2O_4)_3{\cdot}5.5H_2O$ and its calcined samples at different temperatures in air for 1 h

From Fig. 3a, characteristic diffraction peaks of crystalline compound from the precursor are observed, which indicates that the $Cu_{0.5}Mg_{0.5}Fe_2(C_2O_4)_3{\cdot}5.5H_2O$ obtained at 75 °C is a crystalline with higher crystallinity. The diffraction peaks in the pattern can be indexed to be in agreement with the orthorhombic $FeC_2O_4{\cdot}2H_2O$ from PDF card 23-0293, with space group 12/a(15). No diffraction peaks of copper oxalate and magnesium oxalate, such as CuC_2O_4, $CuC_2O_4{\cdot}xH_2O$, MgC_2O_4, and $MgC_2O_4{\cdot}xH_2O$ are observed, which implies that Cu^{2+} and Mg^{2+} ions enter lattice of $FeC_2O_4{\cdot}2H_2O$, and CuC_2O_4, $CuC_2O_4{\cdot}xH_2O$, MgC_2O_4, and $MgC_2O_4{\cdot}xH_2O$ form a solid solution with $FeC_2O_4{\cdot}2H_2O$. It is explained by the fact that Cu^{2+} ion (72 pm), Mg^{2+} ion (65 pm), and Fe^{2+} ion (76 pm) have same electric charge and similar ionic radius. When the precursor is calcined at 300 °C for 1 h, characteristic diffraction peaks of crystalline compound are observed, all the diffraction peaks in the pattern are in agreement with that of cubic $MgFe_2O_4$ [space group Fd-3m(227), PDF card 36-0398] and cubic $CuFe_2O_4$ [space group Fd-3m(227), PDF card 77-0010], which indicates that $MgFe_2O_4$ and $CuFe_2O_4$ in the calcined product $Cu_{0.5}Mg_{0.5}Fe_2O_4$ form a solid solution. Intensity of diffraction peaks of cubic $Cu_{0.5}Mg_{0.5}Fe_2O_4$ increases with increasing calcination temperature, which indicates that crystallite sizes of cubic $Cu_{0.5}Mg_{0.5}Fe_2O_4$ increases with increasing calcination temperature. However, diffraction peaks of impurities, such as CuO, and MgO, increase with increasing calcination temperature, which implies that crystallinity of $Cu_{0.5}Mg_{0.5}Fe_2O_4$ decreases with increasing calcination temperature.

According to the Scherrer formula [11]: $D = K\lambda/(\beta\cos\theta)$, where D is crystallite diameter, $K = 0.89$ (the Scherrer constant), $\lambda = 0.15406$ nm (wavelength of the X-ray used), β is the width of line at the half-maximum intensity, and θ is the corresponding angle. The resulting crystallite sizes of the products from calcining precursor at the temperatures of 400, 600, 700, and 800 °C for 1 h, are 30, 40, 48, and 52 nm, respectively.

4.4 SEM and EDS Analysis of Calcined Samples

The morphologies and EDS spectrum of the calcined samples are shown in Fig. 4. From Fig. 4a, it can be seen that the calcined sample obtained at 600 °C is composed of approximately spherical particles, and there is a soft agglomeration phenomenon in the particles of $Cu_{0.5}Mg_{0.5}Fe_2O_4$ sample, which contains particles having a distribution of small particles (70–100 nm) and large particles (100–200 nm). With the increase of calcination temperature, the calcined sample is aggregated into larger polyhedral grains further. Figure 4c shows the SEM micrograph of sample obtained at 800 °C. It can be seen that the particle sizes of calcined sample obtained at 800 °C are between 250 and 500 nm. The average crystallite sizes of the calcined samples determined by X-ray diffraction are significantly smaller than the values determined by SEM. This is attributed that values observed by SEM technique give the size of the secondary particles, and the X-ray line broadening analysis discloses only the size of primary particles. EDS spectrum of the calcined product at 700 °C shows that the atomic percentages of Cu, Mg, and Fe are 15.36 %, 16.01 %, and 68.63 %, respectively. In other words, that mole ratio of Cu:Mg:Fe in calcined product is equal to 0.47:0.49:2.10, which is close to the value of the pre-design and synthesis.

4.5 Magnetic Properties of Calcined Samples

Figure 5 shows the hysteresis loops of the $Cu_{0.5}Mg_{0.5}Fe_2O_4$ particles obtained at different calcination temperatures. From Fig. 5, it can be observed that specific saturation magnetizations of powders calcined at 400, 600, 700, and 800 °C for 1 h are 25.4, 36.8, 32.5, and 31.7 emu g^{-1}, respectively. That is, specific saturation magnetization increases between 400 and 600 °C with increasing calcination temperature. In other words, the larger the crystallite size of the particles, the larger is the specific saturation magnetizations. The larger M_s values associated with larger crystallite sizes can be explained as follow: First, surface distortions due to the interaction of the transition metal ions with the oxygen atoms in the spinel lattice of $Cu_{0.5}Mg_{0.5}Fe_2O_4$

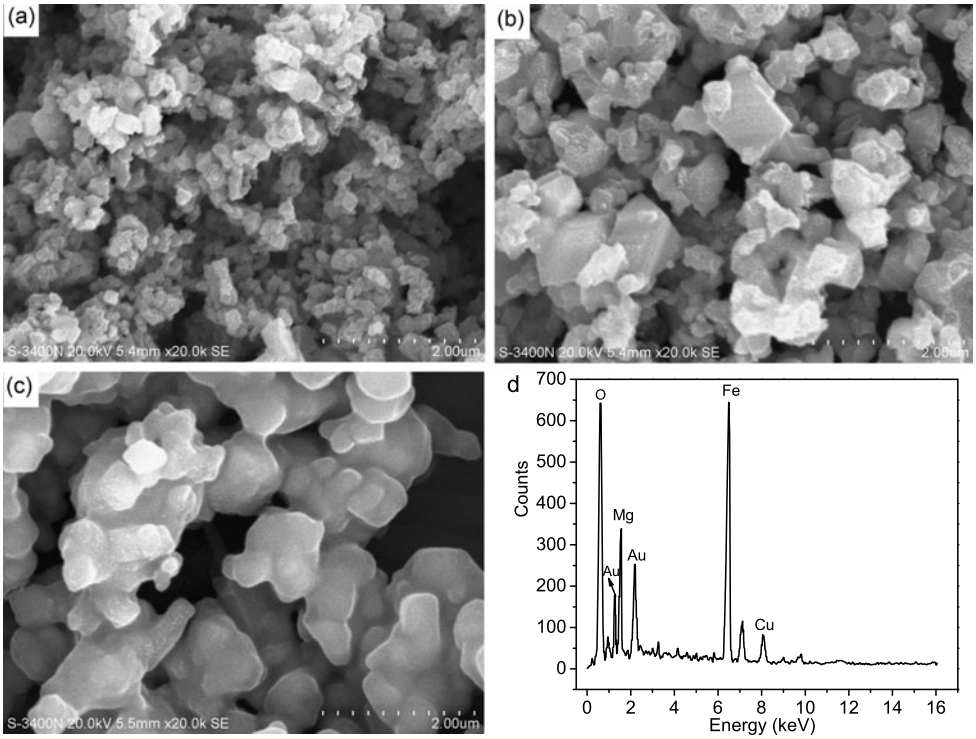

Fig. 4 SEM and EDS analysis of the calcined sample: (**a**) 600 °C, (**b**) 700 °C, and (**c**) 800 °C

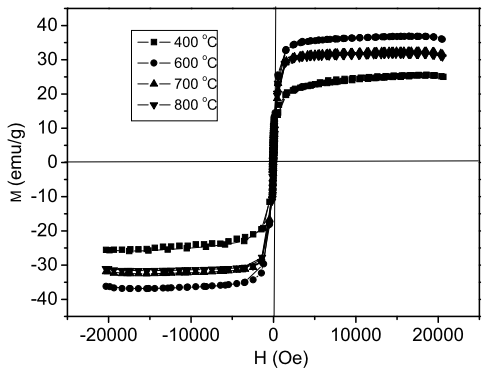

Fig. 5 *M*–*H* (magnetization–hysteresis) loops of $Cu_{0.5}Mg_{0.5}Fe_2O_4$ samples obtained at different temperatures in air for 1 h

can reduce the net magnetic moment in the particle. When the calcination temperature increases, the crystallite size of particles increases, and surface distortions is reduced, so M_s value increases with increasing calcination temperature. Second, the magnetocrystalline anisotropy of the particles is dependent on the crystallinity of $Cu_{0.5}Mg_{0.5}Fe_2O_4$. The higher calcination temperature, the larger is crystallinity of particles, which reduces magnetocrystalline anisotropy distortion, and increases magnetic moment within the particles of $Cu_{0.5}Mg_{0.5}Fe_2O_4$ [3, 11]. Compared with magnetic properties of $CuFe_2O_4$ (600 °C, 33.5 emu g^{-1}) [19] and $MgFe_2O_4$ (600 °C, 30.4 emu g^{-1}) [6], it can be seen that $Cu_{0.5}Mg_{0.5}Fe_2O_4$ obtained at 600 °C exhibits higher specific saturation magnetizations than $CuFe_2O_4$ and $MgFe_2O_4$ obtained at same calcination temperature, which implies that Cu^{2+}, and Mg^{2+} ions in $Cu_{0.5}Mg_{0.5}Fe_2O_4$ have a synergistic effect in improving the saturation magnetization of $Cu_{0.5}Mg_{0.5}Fe_2O_4$. The reason can be explained as follow: First, when Cu^{2+} ions with magnetic moment are partially substituted by Mg^{2+} ions with zero magnetic moment, Mg^{2+} and Cu^{2+} ions occupy tetrahedral A-site together, which reduces the tetrahedral A-site magnetic moment, and results that magnetic moment of $Cu_{0.5}Mg_{0.5}Fe_2O_4$ is greater than that of $CuFe_2O_4$. Second, the magnetic moment of $MgFe_2O_4$ is less than that of $Cu_{0.5}Mg_{0.5}Fe_2O_4$, which is attributed that part of Mg^{2+} ions occupy octahedral B-site in $MgFe_2O_4$, and part of Fe^{3+} ions occupy tetrahedral A-site. This causes that magnetic moment of tetrahedral A-site increases, and magnetic moment of octahedral B-site decreases, so that the net magnetic moment of $MgFe_2O_4$ is decreased.

When precursor is calcined above 600 °C, specific saturation magnetization decreases with increasing calcination temperature, which is attributed that $Cu_{0.5}Mg_{0.5}Fe_2O_4$ is decomposed into CuO, MgO, and Fe_2O_3 particles with weak magnetic intensity above 600 °C. In other words, crystalline $Cu_{0.5}Mg_{0.5}Fe_2O_4$ is thermodynamically more stable at 600 °C.

4.6 Kinetics of Thermal Process of Precursor

In accordance with TG/DSC, FT-IR, XRD, and EDS analysis of $Cu_{0.5}Mg_{0.5}Fe_2(C_2O_4)_3{\cdot}5.5H_2O$ and its calcined prod-

Table 1 Peak temperature (T_P) and kinetic parameters of thermal process of the precursor for the first and second steps obtained from Kissinger method

Heating rates (K mol^{-1})	Step 1				Step 2			
	T_P (K)	E_a (kJ mol^{-1})	ln A	r^2	T_P (K)	E_a (kJ mol^{-1})	ln A	r^2
10	475	85	20.71	0.9940	528	152	34.26	0.9901
15	482				534			
20	489				539			
25	494				541			

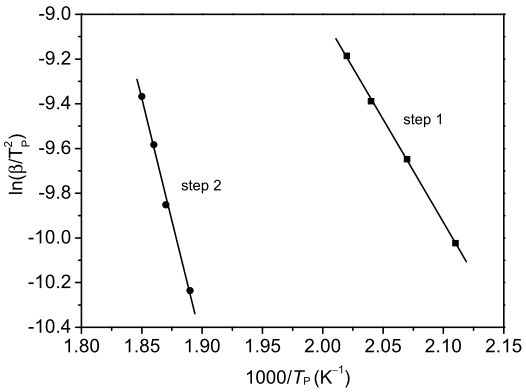

Fig. 6 Kissinger plots of thermal processes of the precursor for the first and second steps

ucts mentioned above, thermal process of the precursor below 700 °C consists of two steps, which can be expressed as follows:

$$Cu_{0.5}Mg_{0.5}Fe_2(C_2O_4)_3\cdot 5.5H_2O(cr) \rightarrow Cu_{0.5}Mg_{0.5}Fe_2(C_2O_4)_3(am) + 5.5H_2O(g) \quad (2)$$

$$Cu_{0.5}Mg_{0.5}Fe_2(C_2O_4)_3(am) + 2O_2(g) \rightarrow Cu_{0.5}Mg_{0.5}Fe_2O_4(c) + 6CO_2(g) \quad (3)$$

Figure 6 shows Kissinger plots of the thermal process of the precursor for the first and second thermal steps. From the slopes of the straight lines, the activation energy values of two thermal process of the precursor are determined to be 85, and 152 kJ mol^{-1} for the first, and second thermal process steps, respectively (Table 1). The step 2 exhibits higher activation energy value in comparison with steps 1, which suggests that thermal decomposition of $Cu_{0.5}Mg_{0.5}Fe_2(C_2O_4)_3$ into $Cu_{0.5}Mg_{0.5}Fe_2O_4$ is the rate-limiting step of the thermal process of the precursor.

5 Conclusions

We have successfully synthesized nanocrystalline $Cu_{0.5}Mg_{0.5}Fe_2O_4$ with cubic structure via a novel and simple method. XRD analysis shows that precursor is a solid solution containing $MFe_2(C_2O_4)_3\cdot 5.5H_2O$ (M = Cu, and Mg). Crystalline $Cu_{0.5}Mg_{0.5}Fe_2O_4$ with cubic structure is obtained via calcining precursor above 300 °C in air for 1 h. Magnetic characterization indicates that the specific saturation magnetization of $Cu_{0.5}Mg_{0.5}Fe_2O_4$ obtained at 600 °C is 36.8 emu g^{-1}. Cu^{2+} and Mg^{2+} ions in $Cu_{0.5}Mg_{0.5}Fe_2O_4$ have a synergistic effect in improving the specific saturation magnetization of $Cu_{0.5}Mg_{0.5}Fe_2O_4$. The thermal process of the precursor in the range of ambient temperature to 700 °C experiences two steps, which involves the dehydration of the five and a half waters of crystallization at first, and then the decomposition of $Cu_{0.5}Mg_{0.5}Fe_2(C_2O_4)_3$ into cubic $Cu_{0.5}Mg_{0.5}Fe_2O_4$. The kinetics of the thermal process of the precursor is studied using DSC technique. The values of the activation energy associated with thermal process of the precursor are 85 and 152 kJ mol^{-1} for the first and second steps, respectively.

Acknowledgements This study was financially supported by the National Nature Science Foundation of China (Grant No. 21161002) and the Guangxi Nature Science Foundation of China (Grant No. 2011GXNSFA018036).

References

1. Maqsood, A., Faraz, A.: J. Supercond. Nov. Magn. doi:10.1007/s10948-011-1343-x
2. Msomi, J.Z., Moyo, T., Abdallah, H.M.I.: J. Supercond. Nov. Magn. doi:10.1007/s10948-011-1235-0
3. Abdallah, H.M.I., Moyo, T., Msomi, J.Z.: J. Supercond. Nov. Magn. **24**, 669–673 (2011)
4. Sun, Z.P., Liu, L., Jia, D.Z., Pan, W.Y.: Sens. Actuators B, Chem. **125**, 144–148 (2007)
5. Li, J.J., Yuan, H.M., Li, G.D., Liu, Y.J., Leng, J.S.: J. Magn. Magn. Mater. **322**, 3396–3400 (2010)
6. Wu, X.H., Wu, W.W., Zhou, K.W., Cui, X.M., Liao, S.: J. Therm. Anal. Calorim. doi:10.1007/s10973-011-1968-9
7. Li, F.S., Wang, H.B., Wang, L., Wang, J.B.: J. Magn. Magn. Mater. **309**, 295–299 (2007)
8. Wu, W.W., Cai, J.C., Wu, X.H., Li, Y.N., Liao, S.: Rare Metals. doi:10.1007/s12598-011-0439-6
9. Satyanarayana, L., Madhusudan Reddy, K., Manorama, S.V.: Mater. Chem. Phys. **82**, 21–26 (2003)
10. Zhang, K., Holloway, T., Pradhan, A.K.: J. Magn. Magn. Mater. **323**, 1616–1622 (2011)
11. Wu, W.W., Cai, J.C., Wu, X.H., Liao, S., Huang, A.G.: Powder Technol. **215– 216**, 200–205 (2012)
12. Goya, G.F., Rechenberg, H.R.: Nanostruct. Mater. **10**, 1001–1011 (1998)

13. Jiang, J.Z., Goya, G.F., Rechenberg, H.R.: J. Phys., Condens. Matter **11**, 4063–4078 (1999)
14. Bomio, M., Lavela, P., Tirado, J.L.: J. Solid State Electrochem. **12**, 729–737 (2008)
15. Pandya, P.B., Joshi, H.H., Kulkarni, R.G.: J. Mater. Sci. Lett. **10**, 474–476 (1991)
16. Tao, S.W., Gao, F., Liu, X.Q., Sørensen, O.T.: Mater. Sci. Eng. B, Solid-State Mater. Adv. Technol. **77**, 172–176 (2000)
17. Zhang, Y., Stangle, G.C.: J. Mater. Res. **9**, 1997–2004 (1994)
18. Vanetsev, A.S., Ivanov, V.K., Tret'yakov, Yu.D.: Dokl., Phys. Chem. **387**, 332–334 (2002)
19. Wu, X.H., Zhou, K.W., Wu, W.W., Cui, X.M., Li, Y.N.: J. Therm. Anal. Calorim. doi:10.1007/s10973-011-2104-6
20. Mathew, T., Shylesh, S., Reddy, S.N., Sebastian, C.P., Date, S.K., Rao, B.S., Kulkarni, S.D.: Catal. Lett. **93**, 155–163 (2004)
21. Birajdar, D.S., Devatwal, U.N., Jadhav, K.M.: J. Mater. Sci. **37**, 1443–1448 (2002)
22. Gabal, M.A., Ahmed, M.A.: J. Mater. Sci. **40**, 387–398 (2005)
23. Banerjee, M., Verma, N., Prasad, R.: J. Mater. Sci. **42**, 1833–1837 (2007)
24. Kenfack, F., Langbein, H.: J. Mater. Sci. **41**, 3683–3693 (2006)
25. Varalaxmi, N., Siva Kumar, K.V.: J. Mater. Sci., Mater. Electron. **22**, 555–560 (2011)
26. Kissinger, H.E.: Anal. Chem. **29**, 1702–1706 (1957)
27. Danvirutai, C., Noisong, P., Youngme, S.: J. Therm. Anal. Calorim. **100**, 117–124 (2010)
28. Boonchom, B., Danvirutai, C.: J. Therm. Anal. Calorim. **98**, 771–777 (2009)
29. Vlaev, L., Nedelchev, N., Gyurova, K., Zagorcheva, M.: J. Anal. Appl. Pyrolysis **81**, 253–262 (2008)